AD-A047 832 NAVAL RESEARCH LAB WASHINGTON D C F/G 20/6
OPTICAL RECORDING CHARACTERISTICS OF KF:LIF PHOTODICHROIC CRYST--ETC(U)
OCT 77 W C COLLINS, M J MARRONE

UNCLASSIFIED NRL-8168 SBIE-E000 070 NL

| OF |
AD
A047832

END
DATE
FILMED
1 -78
DDC

(12)

NRL Report 8168

Optical Recording Characteristics of KF:LiF Photodichroic Crystals

WILLIAM C. COLLINS, MICHAEL J. MARRONE, and MICHAEL E. GINGERICH

Insulator Physics Branch
Material Sciences Division

October 18, 1977

NAVAL RESEARCH LABORATORY
Washington, D.C.

SECURITY CLASSIFICATION OF THIS PAGE (When Data Entered)

REPORT DOCUMENTATION PAGE

READ INSTRUCTIONS BEFORE COMPLETING FORM

1. REPORT NUMBER: NRL [redacted]8168	2. GOVT ACCESSION NO.
3. RECIPIENT'S CATALOG NUMBER	
4. TITLE (and Subtitle): OPTICAL RECORDING CHARACTERISTICS OF KF:LiF PHOTODICHROIC CRYSTALS.	5. TYPE OF REPORT & PERIOD COVERED: Interim report [redacted] continuing NRL Problem.
	6. PERFORMING ORG. REPORT NUMBER
7. AUTHOR(s): William C. Collins, Michael J. Marrone [redacted] Michael E. Gingerich	8. CONTRACT OR GRANT NUMBER(s)
9. PERFORMING ORGANIZATION NAME AND ADDRESS: Naval Research Laboratory, Washington, DC 20375	10. PROGRAM ELEMENT, PROJECT, TASK AREA & WORK UNIT NUMBERS: NRL Problem D03-17F
11. CONTROLLING OFFICE NAME AND ADDRESS: Naval Electronic Systems Command, Washington, D.C.	12. REPORT DATE: Oct [redacted] 77
	13. NUMBER OF PAGES: 33
14. MONITORING AGENCY NAME & ADDRESS(if different from Controlling Office): SBIE; E0001070	15. SECURITY CLASS. (of this report): UNCLASSIFIED
	15a. DECLASSIFICATION/DOWNGRADING SCHEDULE

16. DISTRIBUTION STATEMENT (of this Report)

Approved for public release; distribution unlimited

17. DISTRIBUTION STATEMENT (of the abstract entered in Block 20, if different from Report)

18. SUPPLEMENTARY NOTES

19. KEY WORDS (Continue on reverse side if necessary and identify by block number)

Optical signal processing
Photodichroic crystals
Signal excision
Laser recording

20. ABSTRACT (Continue on reverse side if necessary and identify by block number)

An analysis was made of the optical recording and readout characteristics of the photodichroic KF:LiF crystal containing F_A defects as the activated medium. The results of a series of measurements indicate, in agreement with the analysis, that this crystal system has the highest photosensitivity of any direct reversible recording material without a gain mechanism (≈1 mJ/cm²). The modulation transfer function for a 200-μm-thick activated layer was measured to be 40% at 75 lines/mm, and the dynamic range exceeded 40 dB. The crystal can be operated fatigue free at 220 K by use of thermoelectric → next page

(Continued)

DD FORM 1 JAN 73 1473 EDITION OF 1 NOV 65 IS OBSOLETE S/N 0102-014-6601

SECURITY CLASSIFICATION OF THIS PAGE (When Data Entered)

251950

20. (Abstract) (Continued)

coolers, although optimum performance is predicted for a temperature of about 100 K. The wavelength range of photosensitivity lies in the blue and green and matches the argon laser lines.

CONTENTS

OPTICAL RECORDING CHARACTERISTICS OF KF:LiF PHOTODICHROIC CRYSTALS

INTRODUCTION

Background

A photodichroic material is one which exhibits photo-induced dichroism (absorption of incident light depends on its polarization) and birefringence (velocity of the light in the material depends on its polarization). Alkali halide crystals containing anisotropic defects, which can be aligned along discrete crystallographic directions, are well-known reversible photodichroic materials. Much of the previous work with these materials has dealt with information storage and nondestructive retrieval [1-3]. The M and M_A defects [4,5] are prime candidates for nondestructive readout, but they suffer from one or more problems such as low photosensitivity, inconvenient wavelengths, or severe cooling requirements to avoid fatigue. The F_A defects in KCl:LiCl and KCl:NaCl have also received considerable attention [6]. They have the highest photosensitivity of any photodichroic, but they generally have a destructive readout. Photodichroics have also been used as holographic storage media [7]. Recent emphasis on optical spectrum analysis of raster-recorded signals [8,9] has caused renewed interest in photodichroic materials, since the requirement for a virtual nondestructive read is somewhat relaxed. In this case the signal is recorded by a modulated focused scanning laser beam in a raster format with frame times of a few milliseconds. The Fourier transform can be obtained by uniform illumination so long as the detector used can analyze the spectrum before significant decay of the recorded raster. It may also be necessary to recover the recorded raster from the input transducer after analysis by rescanning, and this must be accomplished before the raster is erased. Alternative input transducers such as the General Electric coherent light valve have no storage facility and cannot accomplish this. In addition to a photodichroic material being used as an input transducer to an optical spectrum analyzer, it has an important potential application in the analysis of these signals in the transform plane [10]. In the spectral analysis of the recorded raster the presence of persistant strong narrow-band sources makes it difficult to detect adjacent weak sources and particularly transient sources. The photodichroic material can operate as a change detector in this case or attenuate long-term strong background signals while transmitting weak adjacent signals. (This application, known as signal excision, is described in Appendix A.) A schematic of both uses of the photodichroic is shown in Fig. 1.

This report describes developmental work on a relatively new photodichroic crystal: F_A defects in KF:LiF. Since the crystal is hydroscopic, special handling is required, but it has many desirable features not shared by other photodichroics. Its photosensitivity is among the highest of all photodichroics, it can be operated fatigue free not far below room temperature using simple thermoelectric coolers in a dry nitrogen atmosphere, and its wavelength range is ideally matched to the strong argon laser lines.

Manuscript submitted August 25, 1977.

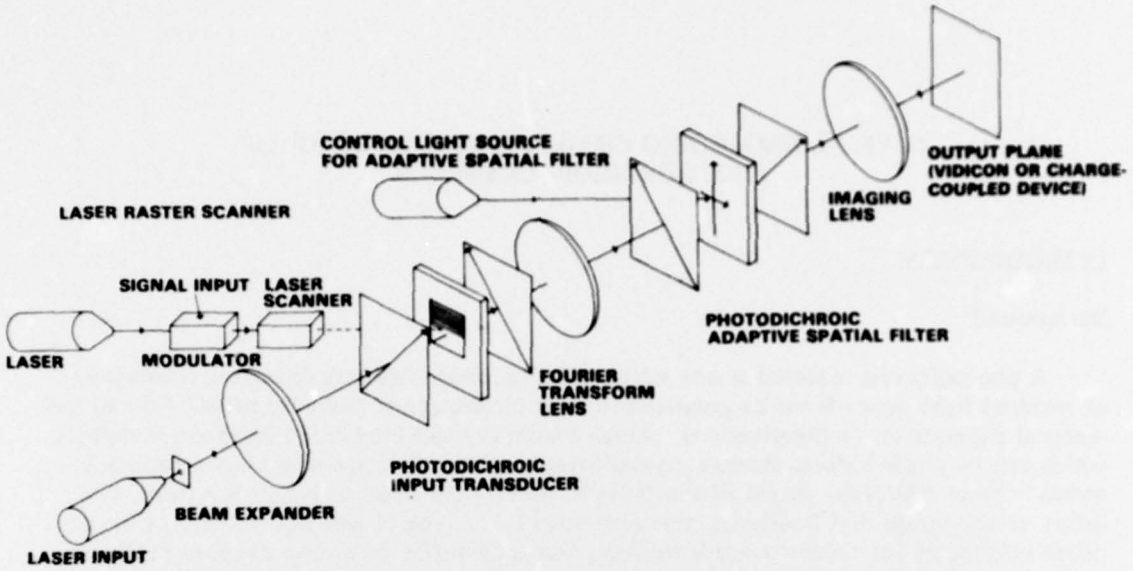

Fig. 1 — Raster-scanned optical spectral analyzer using a photodichroic as an input transducer and as an adaptive spatial filter in the transform plane. The raster scanner is shown off axis, but it could be placed on axis by use of a beamsplitter.

Physics of the F_A Defect

When a normally transparent alkali-halide crystal is exposed to ionizing radiation or heated in an alkali atmosphere, halide vacancies are formed which after trapping an electron can absorb visible light. The crystal is thus colored, and the defects formed are called F centers. The absorption of F centers is isotropic and occurs in a single Gaussian band with no useful properties as a recording medium. However, if the crystal contains alkali impurities of smaller ionic radius than the host (such as the KF:LiF mixture) and the F centers are optically excited at the appropriate temperature, the defects diffuse and become trapped at sites adjacent to the Li^+ sites. The new defects formed are known as F_A centers, and their optical properties are radically altered [11,12]. F_A centers (Fig. 2) are anisotropic, with a triad of optical dipole moments, one being parallel to the vacancy-impurity axis and two being perpendicular to this axis. The usual F-center singlet absorption splits and becomes a doublet corresponding to the triad of optical moments along the crystal $< 100 >$ axis. The moment parallel to the impurity-vacancy axis gives rise to a longer wavelength absorption (F_{A_1}), and the two perpendicular moments are degenerate and give rise to a single shorter wavelength absorption (F_{A_2}). All three moments have equal oscillator strengths.

Thus the F_A absorption consists of a double band whose components partially overlap. In addition, when these F_A defects are optically excited, they can rotate about the Li^+ defect by ionic motion of the halide ions to a new perpendicular orientation with a quantum efficiency of 0.5. As long as the F_A centers have their impurity-vacancy axes randomly oriented (1/3 along each of the three $< 100 >$ directions), the crystal absorbs light isotropically. However if the F_A centers are excited with light in one band exclusively and polarized along the crystal axis, the defects rotate until their optical moment is

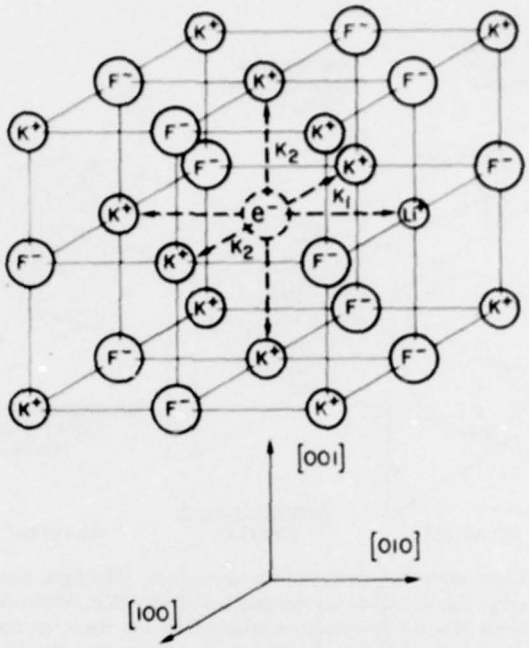

Fig. 2 — The F_A defect in a KF:LiF lattice. This consist of a F^- vacancy which has captured an electron, with a Li^+ nearest neighbor. The three optical dipole moments are shown.

perpendicular to the polarization. Thus the centers can be preferentially aligned. The medium acts as a temporary polarizer to incident light in either of the absorption bands. The polarizing property is lost by randomizing the defect orientations, either by exposing to light whose polarization bisects the crystal axes or using a wavelength which equally excites both absorption bands. Thus the medium behaves as a reversible polarizer whose polarization properties can be spatially and temporally controlled by the polarization of incident light. These properties are best used when the crystal is placed between crossed polarizers whose easy directions are 45° to the crystal axis (Fig. 3). In those areas of the crystal where the defects are randomly oriented, the crossed polarizers extinguish the readout light. For nonrandom orientation the polarization direction of the readout light is rotated in penetrating the crystal, and the analyzer transmits light from that area. The transmission is determined by the relative absorption of light along the crystal axis, that is, by the dichroism induced by nonrandom orientation.

THEORETICAL ANALYSIS

Signal Recording Characteristics

Signals are recorded on a photodichroic crystal by optically pumping anisotropic defects from a random distribution to an aligned distribution as described in Appendix A. The efficiency for inducing alignment is proportional to the difference in the fraction of

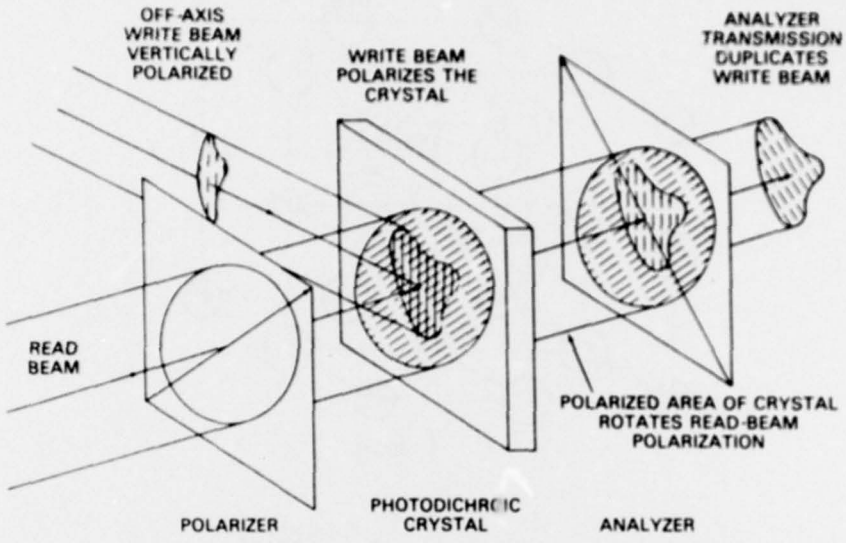

Fig. 3 — Photodichroic recording and reading operations. The light distribution in the write beam modulates the polarization properties of the photodichroic crystal. The uniform readout beam has its polarization rotated in the same pattern as the write beam. Only the rotated parts of the readout beam are thus transmitted by the analyzer. The output light distribution duplicates the write-beam distribution. The off-axis recording beam could be placed on axis by use of a beamsplitter.

incident light (polarized along the crystal axis) absorbed by the components F_{A_1} and F_{A_2}. If the wavelength is such that both bands are equally excited, then no alignment occurs. The wavelength dependence of the recording sensitivity for a KF:LiF crystal at 240 K is shown in Fig. 4.

The dynamic characteristics of the recording medium can be calculated for exposure to light of arbitrary wavelength and polarization. This involves three coupled nonlinear differential equations which are quite complicated. However, for the simple and important case of excitation in one band exclusively and with polarization along the crystal axis, the differential equations simplify and are derived and solved in Appendix B. The solutions for the optical densities measured along the crystal axis are given by Eqs. B12 as

$$K_1(E) = \log\left[(10^{K_0} - 1)e^{-pE} + 1\right]$$

and

$$K_2(E) = \frac{3}{2} K_0 - \frac{1}{2} K_1(E)$$

where K_0 is the initial optical density measured along either crystal axis (assuming initial randomization), E is the exposure in mJ/cm^2, and p is a factor in cm^2/mJ depending on temperature as given in Appendix B. Thus, when a signal is recorded onto a photodichroic, it is stored as a difference in absorption along the crystal axis: $K_1 - K_2$. These calculated recording characteristics are plotted in Fig. 5.

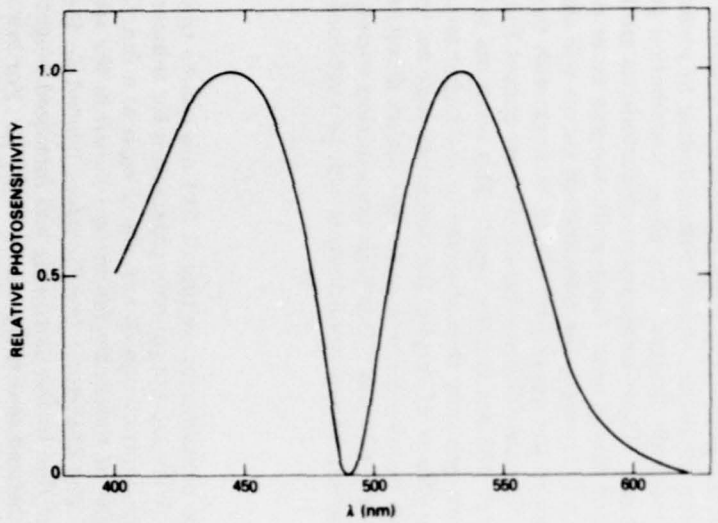

Fig. 4 — Recording sensitivity of a KF:LiF photodichroic crystal at -30°C as a function of wavelength. These characteristics narrow and shift toward the violet when the temperature is lowered.

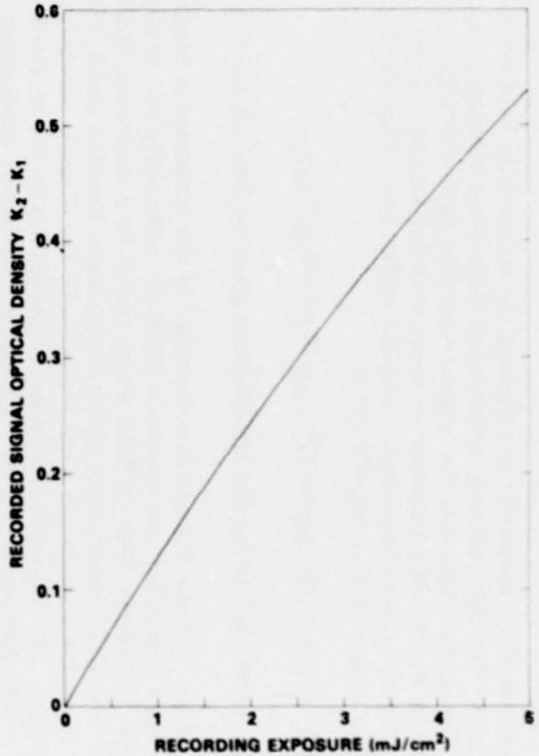

Fig. 5 — Calculated recording characteristics at 514 nm for a KF:LiF crystal at 240 K and an initial optical density of 0.6. The signal is recorded as a difference in optical density along the crystal axis.

Signal Recovery Characteristics

The signal is recovered by uniformly illuminating the crystal with light polarized at 45° to the crystal axis. The light-intensity distribution transmitted through an analyzer on the output side of the crystal duplicates the original recording light distribution, as schematically shown in Fig. 3. The transmission arises from the selective attenuation and rotation of the incident E vector components along the crystal axis. The transmission equation is derived in Appendix C as Eq. C8 and is

$$T = \frac{1}{4}\,(10^{-K_1/2} - 10^{-K_2/2})^2 + 10^{-(K_1+K_2)/2}\sin^2\delta/2,$$

where δ is the phase angle induced by the birefringence given by Eqs. C2 and C3.

This equation states that the absorptive component of the transmission cannot exceed 25% but the phase component can approach 100% for sufficiently low absorption and large phase angle. Of course both of these terms cannot be a maximum simultaneously. Figure 6 shows the wavelength dependence of the transmission function (solid curve in the lower part of the figure) for a saturation write indicated by the dichroic absorption in the upper part of the figure. The absorptive and phase contributions to the transmission function are shown by dotted and dashed curves respectively. The severe attenuation in transmission below 450 nm is due to the higher average absorption in this wavelength range. The transmission at 488 nm is purely due to phase effects, but at 514 nm there is a nearly equal contribution from the absorptive term. The dichroism shown in Fig. 6 was chosen atypically large to illustrate the potentially large transmission available at 488 nm. In Fig. 7 a series of transmission curves are shown corresponding to sucessive changes in dichroism as indicated by the scale changes. The phase contribution grows faster than the absorptive for larger dichroism. These transmission characteristics are for a crystal temperature of 240 K. Since the dichroic bands shift, become more narrow, and increase in height as the temperature is lowered, the transmission curves will change. The dichroic absorption at 77 K is shown in the upper part of Fig. 8 along with the corresponding transmission curve below. The two dichroic bands are now almost fully separated, and the average optical density at 488 nm is quite small. This accounts for the large increase in transmission at this wavelength over that observed in the higher temperature case in Fig. 6. Figure 9 shows the effects of varying the dichroism scale on transmission at 77 K. The transmission at 488 can become quite large for the higher densities. The transmission is still significant out to nearly 600 nm. This high transmission corresponding to large dichroism is obtained at the expense of resolution, as will be explained later.

Dynamic Characteristics

The complete dynamic behavior for writing at 514 nm can be obtained by substituting Eqs. B12 into Eq. C8. With the appropriate parameters for temperature and initial optical density this gives the transmission at any wavelength as a function of the laser energy exposure. The results of these calculations are shown in the series of log-log plots of Figs. 10a through 10d. The changes in the K_0 values labeled on the curves from the 240-K to the 77-K plots are due to the narrowing and increased height of the bands. This accounts in part for the enhanced sensitivity shown at 77 K. For low exposures all of these curves are approximately linear in amplitude transmittance. However there are significant dynamic differences between the 514-nm and 488-nm readouts for changes in

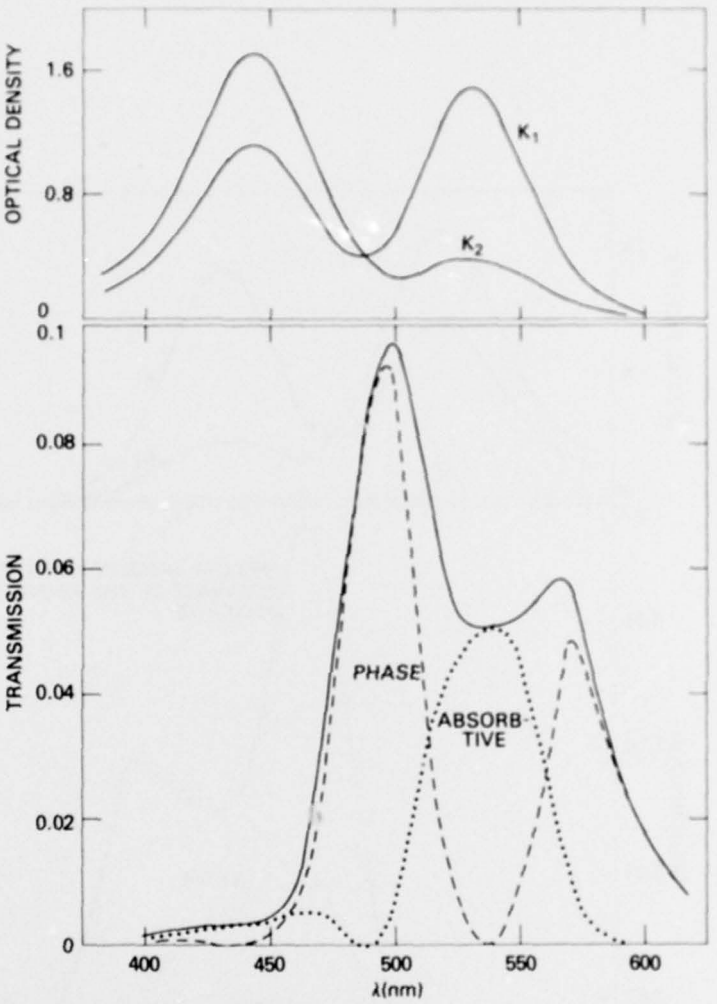

Fig. 6 — Readout transmission characteristics at 240 K for the photo-induced dichroism shown at the top of the figure for a 514-nm write to saturation. The dashed curve and the dotted curve give the phase and the absorptive components of the transmission respectively.

the parameter K_0. This is most evident in the 514-nm readouts at 77 K (Fig. 10c). The slopes change as the value of K_0 is changed, in contrast to the 488-nm curves (Fig. 10d). The origin of this behavior lies in the difference in dynamic behavior between the phase and absorptive components of the transmission. Since the 514-nm readout is composed of a mixture of these effects, its dynamic characteristics are more complicated.

The difference in dynamic behavior between the 514-nm and 488-nm readouts is illustrated by plotting $d\sqrt{T}/dE$ vs exposure. For maximum linearity these functions should be nearly constant with exposure. The results of the calculations are shown in Figs. 11a through 11d. These graphs illustrate more clearly how the linearity and sensitivity change with changes in the initial optical density K_0. The linearity changes with

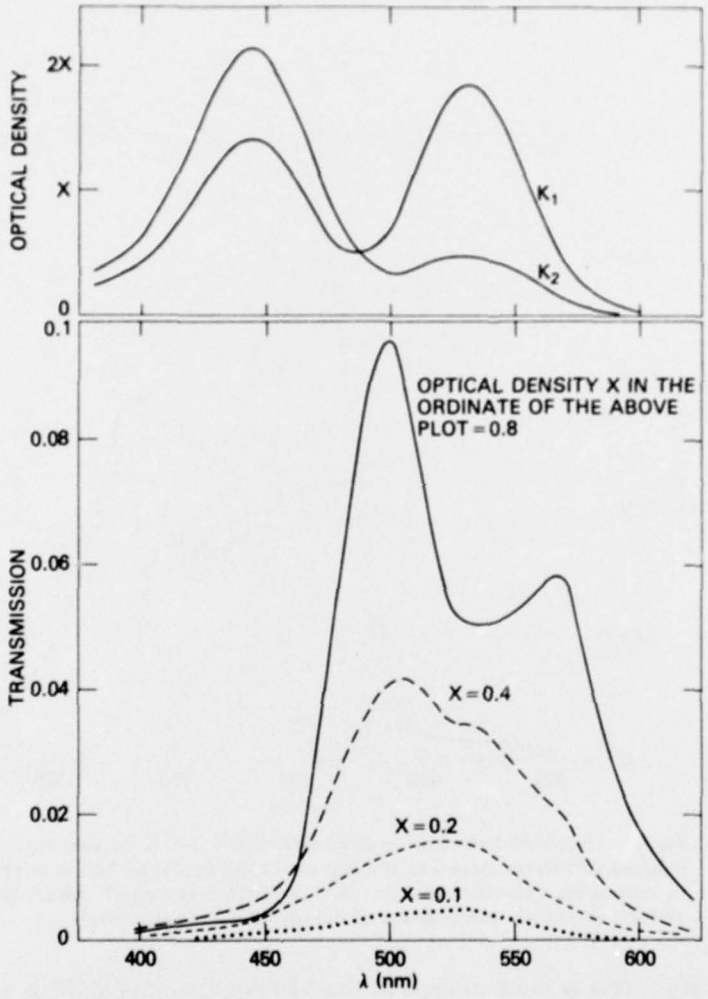

Fig. 7 — Readout transmission characteristics at 240 K for the photo-induced dichroism shown at the top of the figure for a 514-nm write to saturation. The effects on transmission of changes in the optical-density scale are shown.

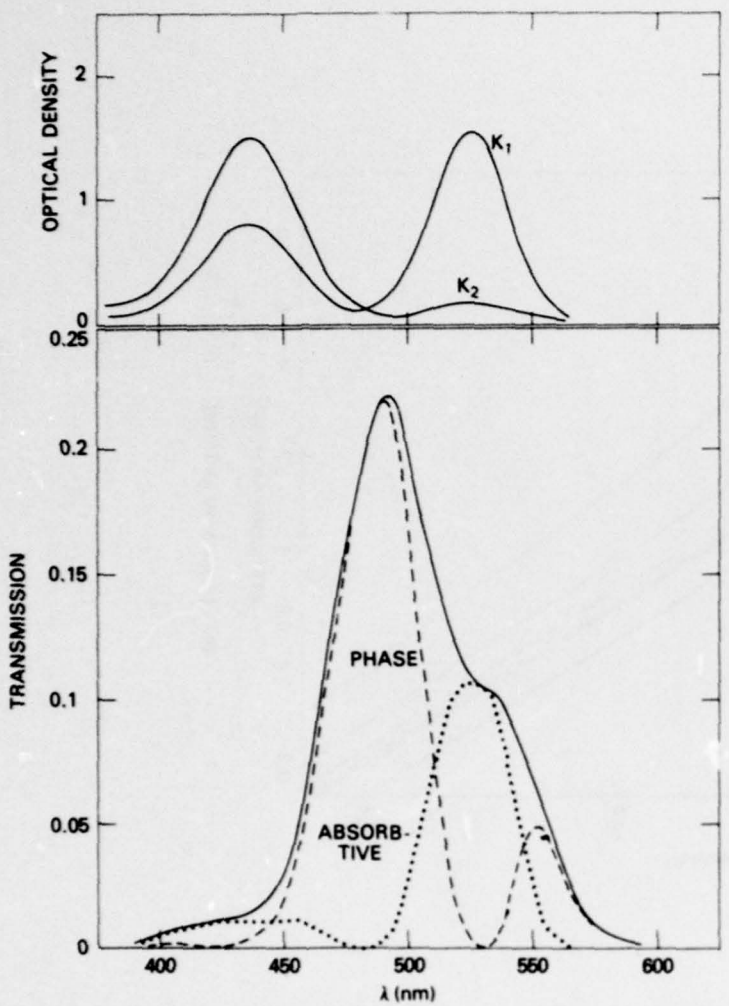

Fig. 8 — Readout transmission characteristics at 77 K for the photo-induced dichroism shown at the top of the figure for a 514-nm write to saturation.

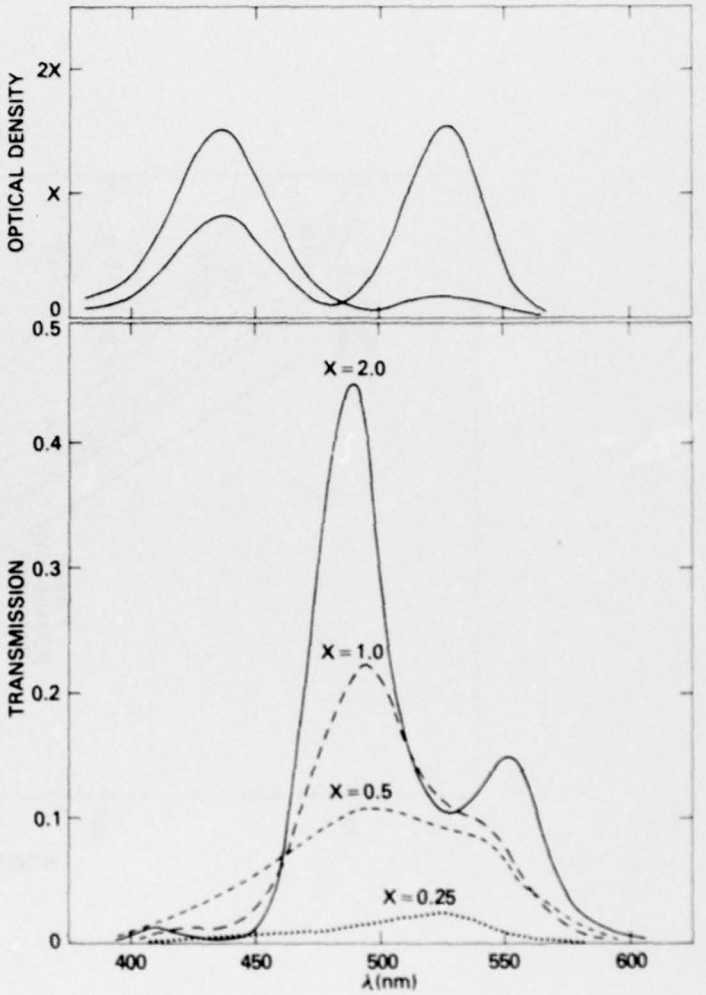

Fig. 9 — Readout transmission characteristics at 77 K for the photo-induced dichroism shown at the top of the figure for a 514-nm write to saturation.

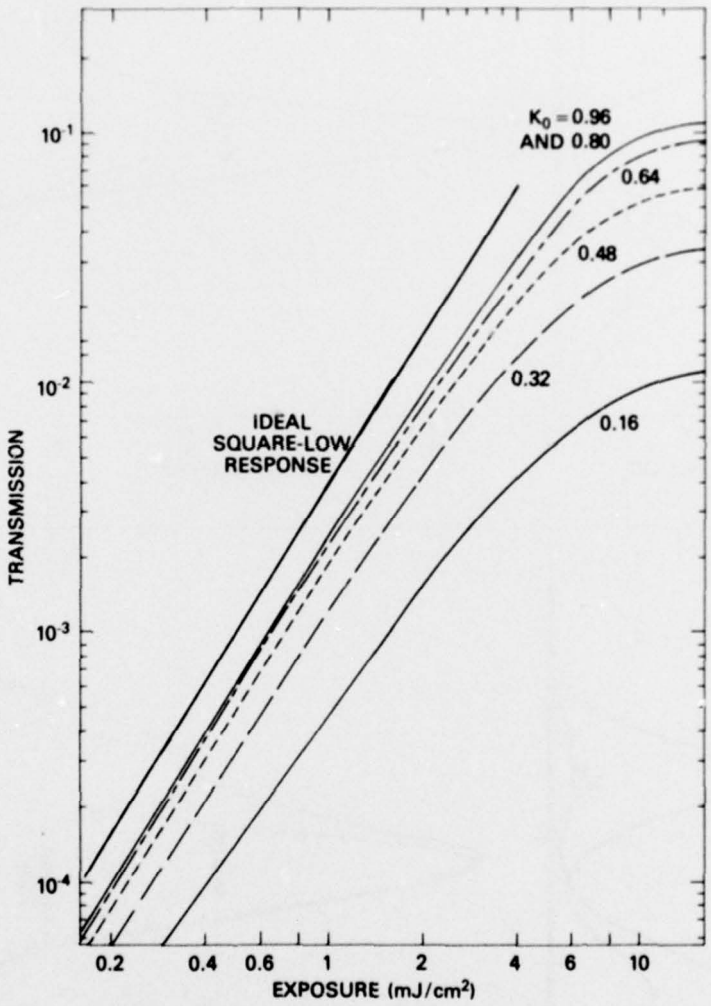

(a) 514-nm read at 240 K

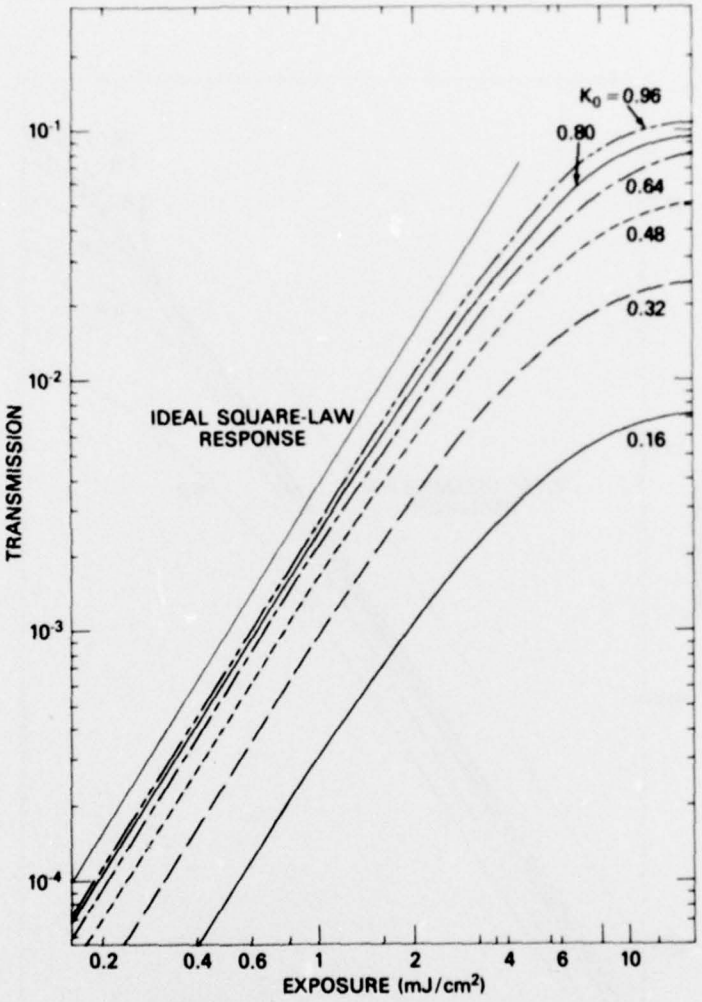

(b) 488-nm read at 240 K

Fig. 10 — Readout transmission vs input exposure calculated from Eqs. B12 and C8 for 514-nm write and the indicated crystal temperature and read wavelength. The upper straight line indicates a slope of 0.5 in each log-log plot, which corresponds to an ideal square-law response (Continued).

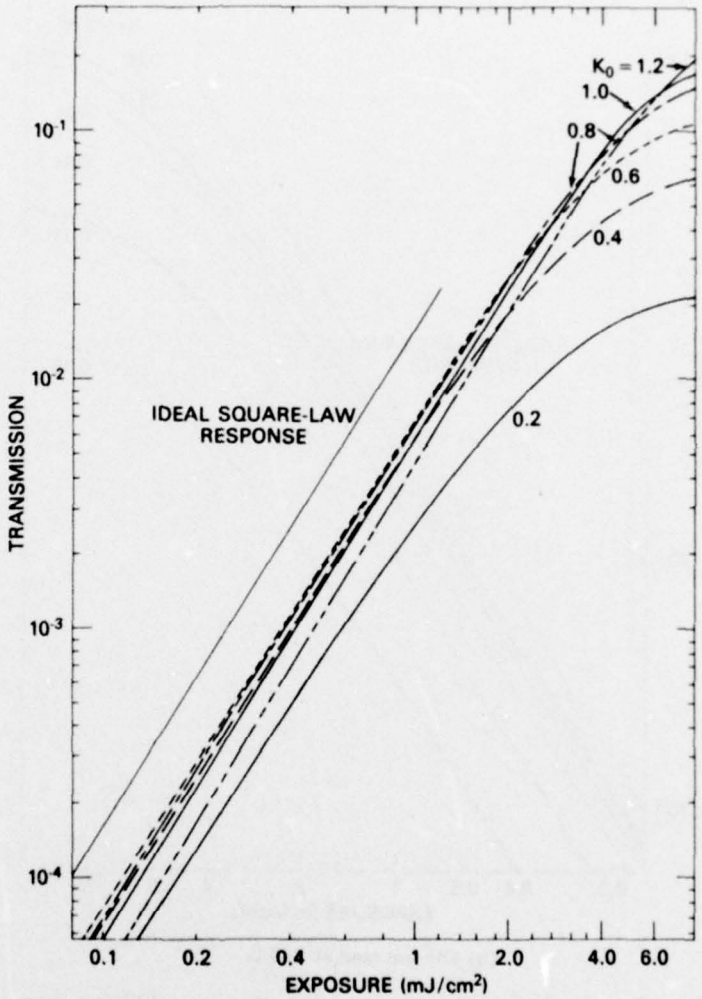

(c) 514-nm read at 77 K

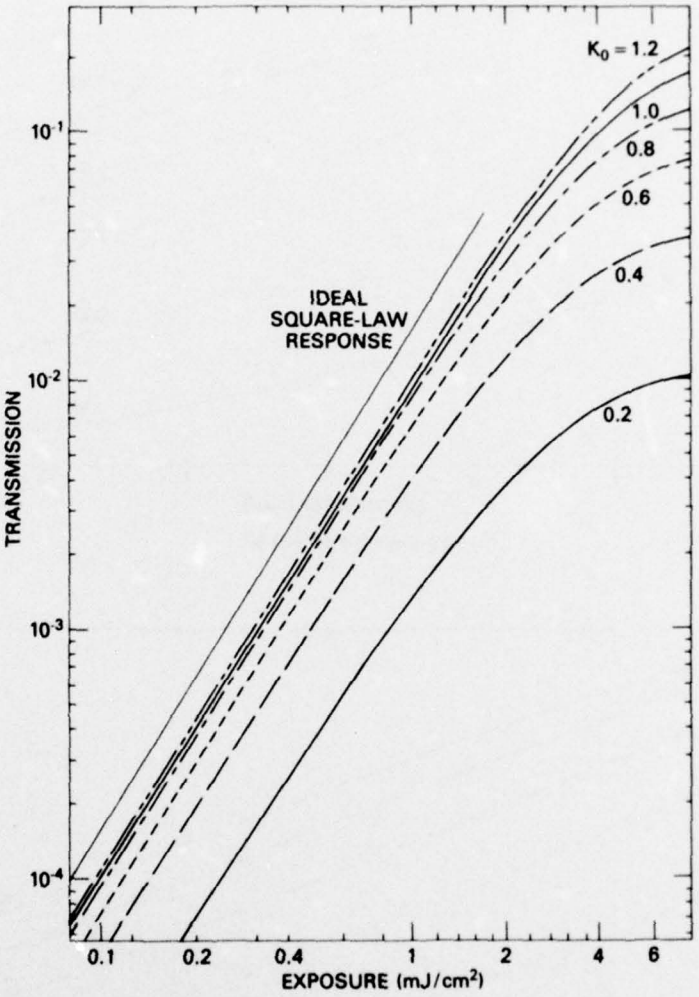

(d) 488-nm read at 77 K

Fig. 10 — Readout transmission vs input exposure calculated from Eqs. B12 and C8 for 514-nm write and the indicated crystal temperature and read wavelength. The upper straight line indicates a slope of 0.5 in each log-log plot, which corresponds to an ideal square-law response (Continued).

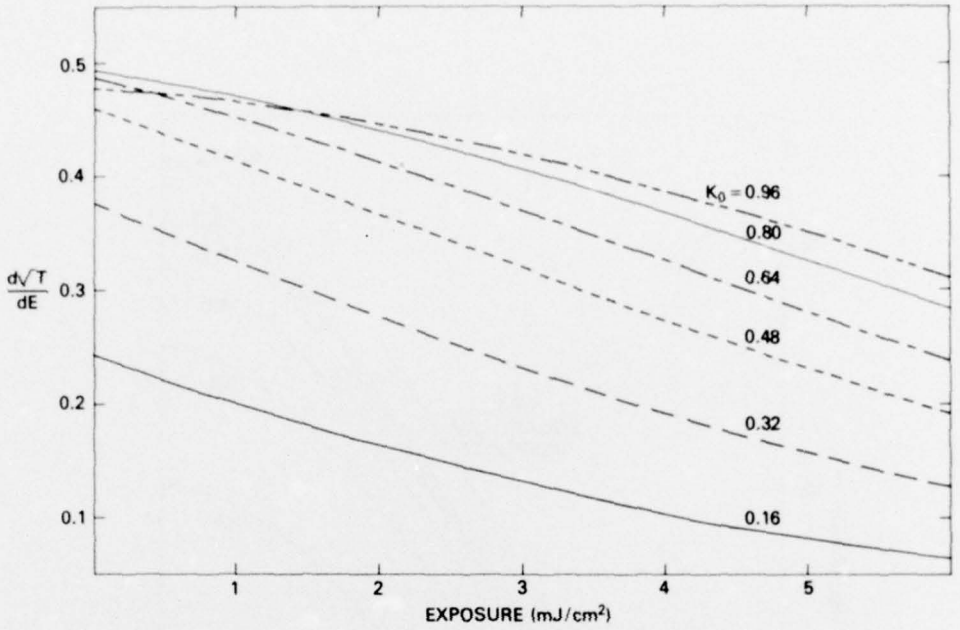

(a) 514-nm read at 240 K

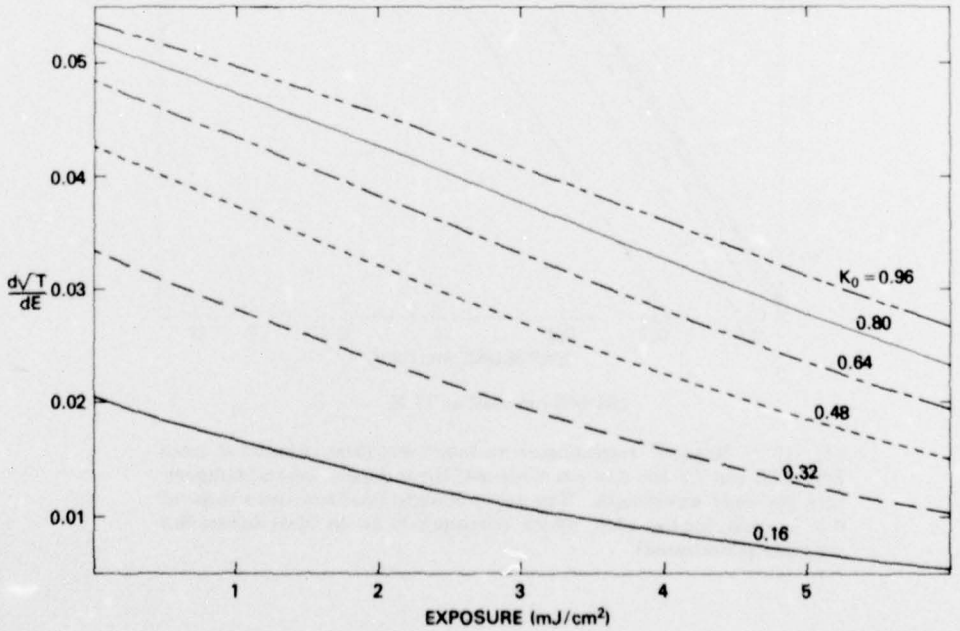

(b) 488-nm read at 240 K

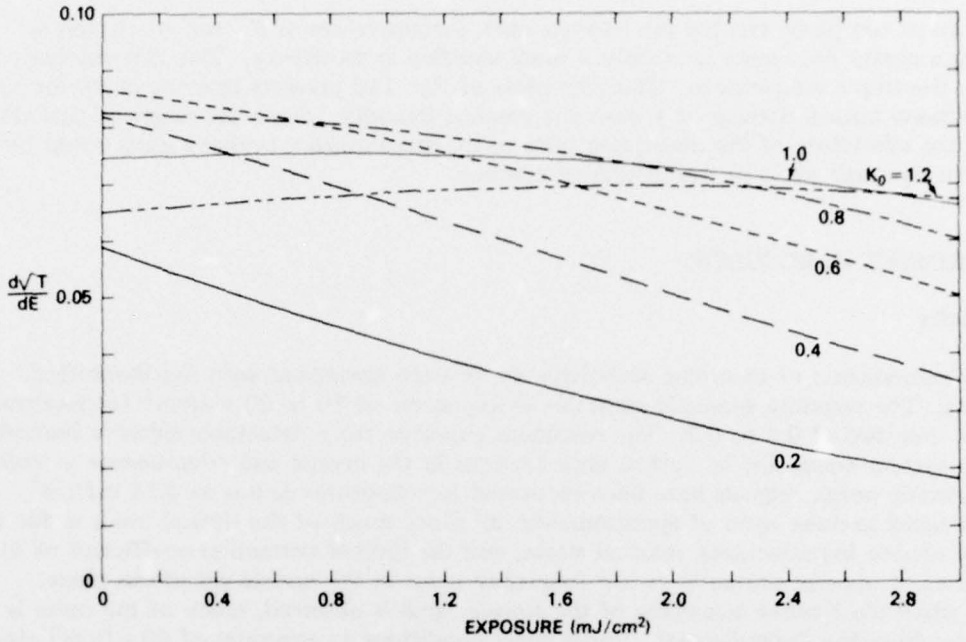

(c) 514-nm read at 77 K

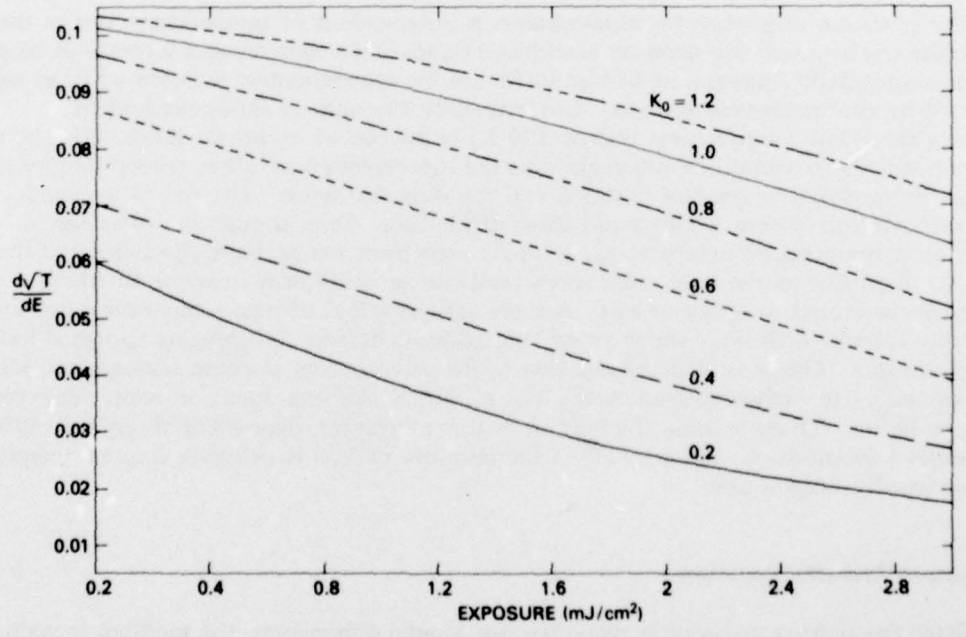

(d) 488-nm read at 77 K

Fig. 11 — Derivative of the amplitude transmittance vs exposure, calculated from Eqs. B12 and C8 for 514-nm write at the indicated crystal temperature and read wavelength (Continued)

K_0 in all of the plots, but for the 514-nm read, certain values of K_0 can be chosen to achieve a nearly flat response at only a small sacrifice in sensitivity. This is particularly true at the lower temperature. Thus the plots of Fig. 11d predicts that the curve for an approximate optical density of 1 gives the greatest linearity. Since the origin of this effect lies in the admixture of the absorptive term in the transmission, similar results could be achieved by small shifts in wavelength of readout.

EXPERIMENTAL RESULTS

Sensitivity

Measurements of recording sensitivity are in close agreement with the theoretical analysis. The response generally saturates at exposures of 10 to 20 mJ/cm^2 for moderate optical densities of 0.4 to 0.6. The minimum exposure for a detectable signal is limited by the system noise, due to optical imperfections in the crystal and components as well as electronic noise. Signals have been recovered for exposures as low as 0.14 mJ/cm^2 with a signal-to-noise ratio of approximately 2. Since much of the optical noise is due to crystal surface imperfections, residual strain, and the limited extinction coefficient of the polarizers, it appears primarily as low-frequency noise in the optical transform plane. Thus, when the Fourier transform of the stored signal is observed, much of the noise is removed from the desired signal. Under these conditions an exposure of 60 μJ/cm^2 gives a detectable signal. With sufficient optical quality this value should also apply to signals recovered from the image plane.

The quantum efficiency for reorientation is independent of temperature; but as the temperature is lowered, the dichroic absorption bands shift, narrow, and increase in height. The photosensitivity increases at 514 and 488 nm by approximately a factor of 2, as was predicted by the theoretical analysis. Unfortunately the only available method of achieving these low temperatures (below 100 K) is the use of cryogenic fluids. The boiling fluid introduces vibrations which prevent the measurement of other critical parameters such as the modulation transfer function and the dynamic range. The use of a closed-cycle refrigeration system would avoid these difficulties. Even though the quantum efficiency is temperature independent, at sufficiently high temperature the relevant defects began to thermally reorient and near room temperature this limits the time to which signals can be stored to a day or less. A more serious effect of high-temperature operation lies in the thermal diffusion, which causes the relevant defects to aggregate and thus lose their dichroism. This loss of dichroism due to diffusion occurs at room temperature after approximately 10^5 write-and-read cycles, but at 240 K this loss does not occur until 10^8 cycles or better. There is some fluctuation in this parameter, depending on crystal purity and defect concentration, but generally a temperature of 220 K or lower assures operation that is virtually fatigue free.

Modulation Transfer Function

Since the defects involved in recording are atomic dimensions, the medium is grainless and the resolution is inherently diffraction limited. However, when used with low-f-number optics, the thickness of the activated volume must not greatly exceed the depth

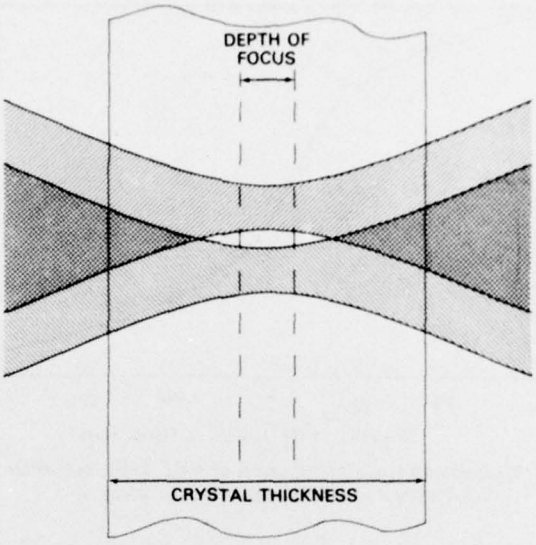

Fig. 12 — The recording of two focused spots of light separated by the spot diameter (Raleigh criterion for resolution) inside a crystal when the crystal thickness *exceeds the depth of focus. Even though* the beams overlap inside the recording medium, the spots can still be resolved on readout due to the higher writing intensity inside the depth of focus, although with a lower modulation transfer function. The diagram is highly exaggerated for illustration.

of focus of the optics. For an f/8 system with a spot size of 5 μm (100 lines/mm) the depth of focus is approximately

$$d = 2(\text{f number})(5\ \mu\text{m}) = 80\ \mu\text{m}. \tag{1}$$

If the crystal thickness exceeds this, the modulation transfer function (MTF) will decrease due to the overlap of the light cone away from focus, as shown in Fig. 12. The MTF can still be significant even for large variations from Eq. 1 due to the higher recording intensity at the waist, where there is no overlap.

A typical MTF curve is shown in Fig. 13 for a crystal with an active thickness of 200 μm. A depth of focus of 200 μm corresponds to a spot size of 12 μm, or a resolution of 40 lines/mm. The MTF should begin to drop at this frequency, and Fig. 13 confirms this. The drop is rather rapid between 40 and 70 lines/mm, but there is a long slowly decreasing tail out to beyond 120 lines/mm, which corresponds to the high-intensity recording at the beam waist.

These measurements were made by several techniques. The simplest method involved recording the image of a bar chart onto the crystal and recovering the stored image onto photographic film after 40× magnification. The MTF was obtained from the film with a microdensitometer. A second technique involved recording an 8-to-12-line/mm Ronchi grating onto the crystal and observing the Fourier transform of the stored grating.

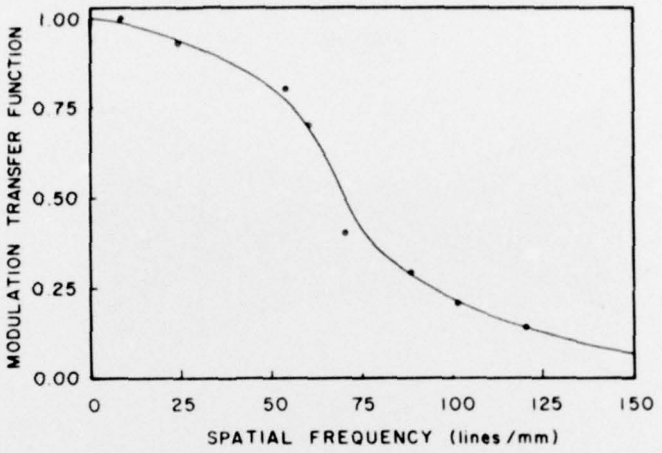

Fig. 13 — Modulation transfer function of a KF:LiF photodichroic crystal with a recording thickness of 200 μm

By comparing the relative magnitude of the diffraction orders with that of the original grating, the MTF is obtained. A third technique involved exposing the crystal to a scanning modulated laser beam and recovering the stored signal with uniform illumination onto photographic film. The MTF was obtained from the film with a microdensitometer.

Linear Dynamic Range

The dynamic range is limited for large-signal recording by nonlinearity and for small-signal recording by the noise generated by surface imperfections and bulk strain. Since the material fabrication is still in an early stage of development, the optical quality of the surfaces and the strain were such that noise prevented the detection of nonlinearity for the lowest exposures (below 2 mJ/cm^2). Hence the dynamic-range data presented are a measure of the lower limit for low exposures and are more accurately a measure of linearity for the higher exposures.

A sinusoidal grating of 30 lines/mm was recorded onto a crystal by interfering two collimated laser beams at 514 nm. The Fourier transform of the recorded grating was detected by a vidicon with a line-scan output. Nonlinear recording is indicated by the presence of a second order in the transform plane. By measuring the ratio of the intensity of the first order to that of the second order, the linear dynamic range in the transform plane is obtained. Two sequences of measurements were performed. One involved using nearly full modulation ($\approx$80%) and varying the basis level, and the other involved varying the bias but keeping the modulation fixed at 0.4 mJ/cm^2. The results of the first measurements are shown in Fig. 14a. The second order was below the noise in the data for exposures below 2 mJ/cm^2; hence a 40-dB linear dynamic range must be considered a lower limit. With improved surface conditions and strain-free crystals the dynamic range should exceed 40 dB. The linearity decreases monotonically for increasing exposure with 80% modulation. Also shown is the signal amplitude transfer function (from Eqs. B12 and C8), indicating the degree of modulation. In the second measurement the bias level was varied but the modulation was fixed at 0.4 mJ/cm^2. These results are shown in Fig.

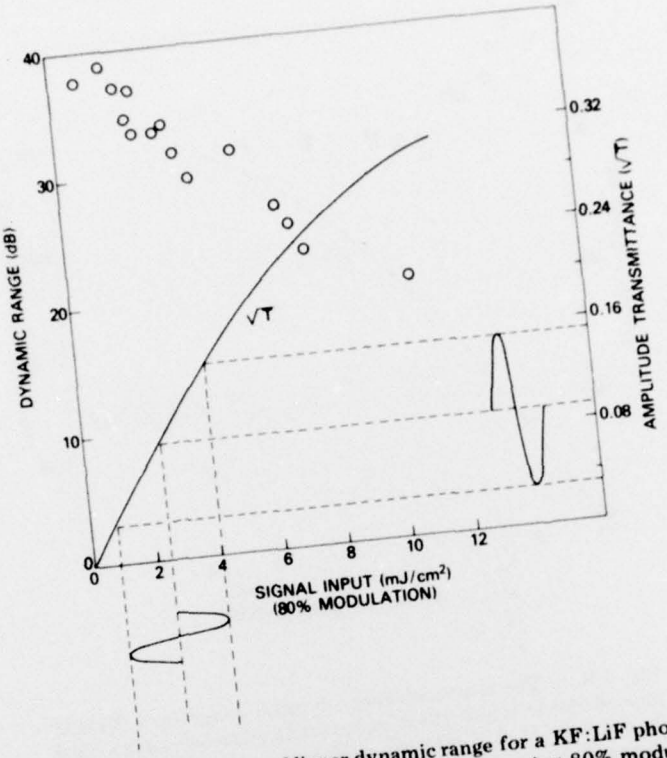

Fig. 14a — The measured linear dynamic range for a KF:LiF photodichroic as a function of recording exposure using 80% modulation. Also shown is the amplitude transmittance from Fig. 10a, indicating the modulation and bias.

14b, along with the amplitude transfer function indicating the modulation used. This indicates that at least 30 dB dynamic range is achieved, even at large exposures, so long as the modulation is small. Again the values measured for small exposures are noise limited. Also, according to the previous analysis, further improvements in dynamic range could be expected by lowering the operating temperature.

Measurements of dynamic range in the image plane are severely restricted by the extinction coefficient of the polarizers as well as any residual strain in the crystal. In the Fourier plane these imperfections are not as severe, since they appear primarily as low-frequency noise. Values of 20 dB were measured for the dynamic range in the image plane, but this should be considerably improved with better crystal quality.

CRYSTAL PREPARATION

Experience in preparation and growth of the KF:LiF mixture (approximately 0.5% LiF) is more limited than that of the more common alkali halides, due to the crystal's hydroscopic nature. Since the starting material absorbs moisture easily, extreme care is required in material preparation before growth of the single crystal. All handling of the crystal after growth must be in a low-humidity atmosphere (below 8%). The experienced

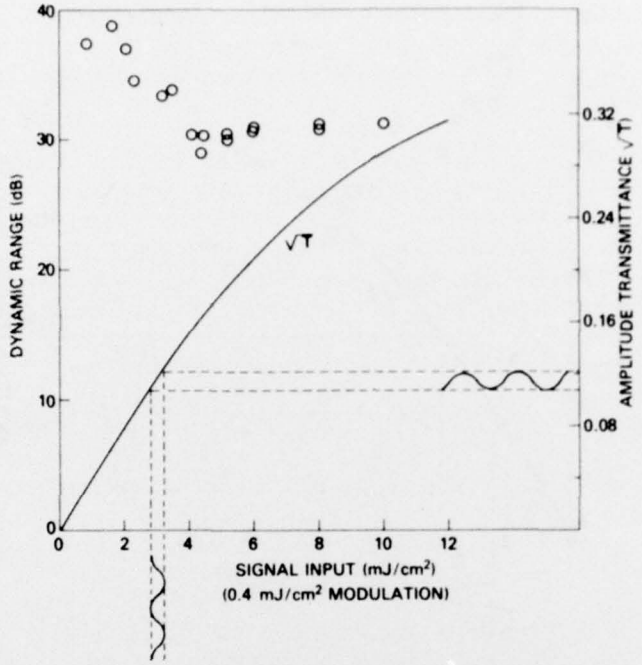

Fig. 14b — The measured linear dynamic range for a KF:LiF photodichroic as a function of recording exposure using a fixed modulation of 0.4 mJ/cm^2. Also shown is the amplitude transmittance from Fig. 10a, indicating the modulation and bias.

sources for KF:LiF are NRL's Electronic Materials Technology Branch, Cornell University's crystal-growth facility, and The University of Utah's crystal-growth facility. The latter source has produced the most-strain-free crystals of the highest optical quality to date and is the major supplier. The usual cross section of these single-crystal boules is approximately 6 cm^2, but they can be grown much larger.

Upon receipt the single-crystal boules are carefully cleaved (to avoid straining) into slabs approximately 3 mm thick. Since the KF:LiF crystals are moderately radiation hard, it is difficult to introduce a high concentration of F_A defects, and special treatment is required: an anneal of the 3-mm slabs at 700°C in a mixed hydrogen and K^+ atmosphere. This treatment causes H^- ions to diffuse into the lattice and substitute for the F^- ions. The concentration of H^- ions depends on the hydrogen pressure (normally 5 atmospheres), and the penetration depth depends on the temperature and annealing time. A 4-hour anneal at 700°C gives a penetration of approximately 200 μm. In this surface layer the crystal composition is KF:LiF:KH. After the anneal, the crystals must be cooled under precise control (10°C/mm). Thermal strain is introduced if the cooling is too fast, and phase separation of the KF:LiF mixture occurs if the cooling is too slow. After the 3 mm slabs are cooled, they are cleaved so that only one surface is composed of KF:LiF:KH. Then the crystals are polished and are sealed between glass flats using an optical grade silicone-rubber compound to protect the surfaces from moisture. This latter technique has been used for convenience in the early developmental stage but introduces

multiple reflections due to index-matching problems. A superior technique would be to sputter SiO_2 or evaporate MgF_2 films of 0.5 to 0.1 μm depth. Preliminary tests indicate the feasibility of achieving layers of this thickness, provided the crystal surfaces are of sufficiently good quality.

Once the crystals are polished and sealed, they are exposed to ionizing radiation. The substitutional H^- ions are easily driven out of their lattice sites, and they combine, forming stable H_2 molecules. These molecules are outgassed from the crystal, leaving behind negative-ion vacancies which trap electrons (F centers). The final step involves exposing the crystals to blue light near room temperature. This causes the F centers to diffuse, until they become trapped at Li^+ sites, thus forming the relevant F_A centers.

The crystals are now ready to be used after cooling to at least -30°C to avoid fatigue problems. They are currently being cooled with a two-stage thermoelectric cooler after being sealed in a dry nitrogen atmosphere. The required cooling is close to the limit for this type of cooler. However optimum performance in terms of sensitivity and dynamic range will occur near 100 K. Hence a closed-cycle refrigeration system would be required. Sensitivity should improve by a factor of 2, and the dynamic range should improve to better than 50 dB. The analysis of performance at low temperature is under way.

An important area of material improvement involves increasing the concentration of defects. This would allow thinner layers of activated defects and thus allow higher resolution. Currently the maximum concentration of stable defects achieved is approximately 10 to 15 parts per million. It should be possible to increase this by several factors before exceeding the solubility limit of LiF in KF.

CONCLUSIONS

The characteristics of the KF:LiF photodichroic crystal make it a leading candidate for use as an input transducer or adaptive spatial filter in an optical spectrum analyzer. It is less sensitive than the electrooptic photoconductors but has much better resolution. Even so the sensitivity is adequate for real-time recording using currently available argon lasers. Since the material is still in an early stage of development, improvements are to be expected in crystal quality which will extend the dynamic range beyond the present 40 dB, which is adequate for many applications. Since the material records with maximum quantum efficiency, no improvement in the inherent sensitivity can be anticipated. However, by use of low-temperature housing, the relevant bands can be made to shift for maximum use of the 514-nm argon line, thus improving the photosensitivity by at least a factor of 2. A second area of improvement lies in the increase in concentration of the F_A defects, which will allow thinner coloration layers. This will improve resolution, and a modulation transfer function of 50% at 150 lines/mm appears feasible.

REFERENCES

1. I. Schneider, M. Marrone, and M. Kabler, *Appl. Opt.* 9, 1163 (1970).
2. J. Burt, H. Knoebel, V. Krone, and B. Kirkwood, *Appl. Opt.* 12, 1213 (1973).

3. W. C. Collins, I. Schneider, M. E. Gingerich, and P. Klein, "Information Storage in Photodichroic Crystals," NRL Memorandum Report 2858, Aug. 1974.

4. I. Schneider, M. Lehmann, and R. Bocker, *Appl. Phys. Letters* **25**, 77 (1974).

5. D. Casasent and F. Caimi, *Appl. Optics* **15**, 815 (Mar. 1976).

6. F. Lanzl. U. Röder, and W. Waidelich, *Appl. Physics Letters* **18**, 56 (Jan. 15, 1971).

7. H. Blume, T. Bader, and F. Lüty, *Opt. Commun.* **12**, 147 (1974).

8. C. E. Thomas, *Appl. Opt.* **5**, 1782 (1966).

9. D. Casasent and F. Casasayas, *Appl. Opt.* **14**, 1364 (1975).

10. W. C. Collins and M. J. Marrone, *Appl. Phys. Letters* **28**, 260 (1976).

11. F. Lüty, pp. 181-242 in *Physics of Color Centers*, edited by W. B. Fowler, Academic Press, New York, 1968.

12. W. C. Collins, and I. Schneider, *J. Phys. Chem. Solids*, **37**, 917 (1976).

Appendix A

SIGNAL EXCISION

The characteristics of the KF:LiF photodichroic when used as a signal excisor in the frequency plane of an optical spectrum analyzer will be described in this appendix. Such an arrangement would appear as shown in Fig. A1. In an optical spectrum analyzer the frequency spectrum of an input temporal signal appears as spots of light in the transform plane. In the analysis of wide-band signals the presence of persistent strong narrowband sources makes it difficult to detect adjacent weak ones. The photodichroic will act as a change detector in this situation and will attenuate long-term strong sources while transmitting weak ones.

Although there are many possible configurations, the arrangement shown in Fig. A1 is typical. Here the crystal is placed in the transform plane, and the dark spots along the X axis on the crystal illustrate the presence of five signals of various intensities. These light spots are polarized at 45° to the crystal axis. The indicated control light would be any broadband blue source which is vertically polarized. A typical sequence might be as follows: The control light source uniformly polarizes the crystal with the signal from the input off. At $t = 0$ the input signal is allowed to fall on the crystal as shown in Fig. A1. At this instant all signals are transmitted with no change in their relative intensity. However, since the signal polarization bisects the crystal axes, there is a randomizing effect and thus a loss of dichroism in these exposed areas. The transmission decay is purely a function of the cumulative energy of exposure, so the area exposed to the central intense light decays much more rapidly than the weakly exposed areas. After a certain time t_1 which depends solely on the peak intensity, the strong signal is suppressed much more severely than the weaker ones, as shown in the reimaged output plane.

The precise decay characteristics depend on the initial optical density, the initial degree of alignment, the temperature, and the wavelength, but a typical set of decay curves is shown in Fig. A2. If the crystal is exposed to uniform light with the indicated intensities, the transmission of light from that area will decay as shown. In the insert a Gaussian beam profile is shown. If the crystal is exposed to such a beam profile, the peak will decay as curve A and the annular ring at B will decay as curve B., etc. out to the low-intensity wings. Thus after a certain exposure such a Gaussian beam would appear as a weak annular ring of light.

The magnitude of the final decrease in transmission is ultimately limited by the extinction coefficient of the crossed polarizers, which can be from 10^{-5} to 10^{-6}. After a few milliseconds of exposure (for a peak intensity of $20 W/cm^2$), the signal source is cut off, the control light source realigns the crystal, and the system is ready to be recycled. Close to a 100% duty cycle is possible, if both signal and control light sources are of sufficient intensity.

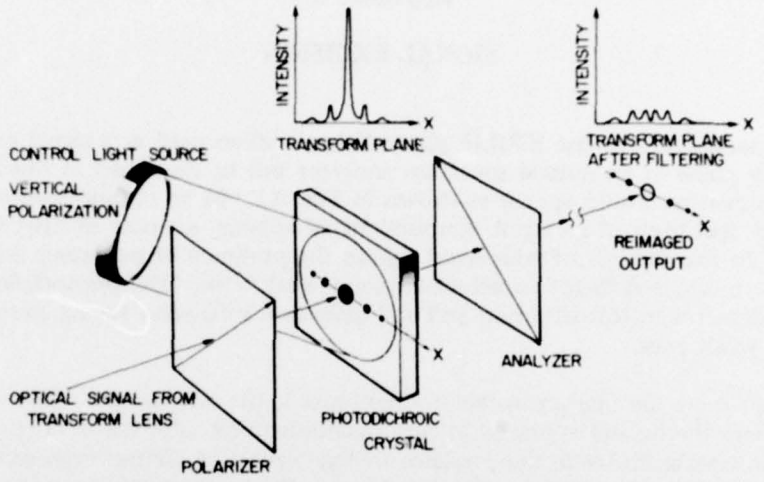

Fig. A1 — Illustration of the photodichroic crystal used as a signal excisor in the frequency plane of an optical spectrum analyzer

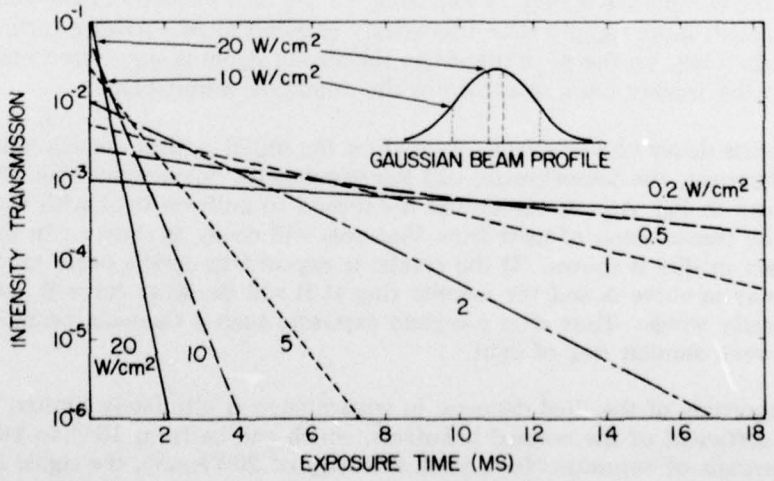

Fig. A2 — Typical decay curves for light-transmission decay through a photodichroic crystal when used in the signal excision mode

Appendix B

REORIENTATION CHARACTERISTICS

To fully understand the recording mechanism of the crystal, the reorientation characteristics must be examined. Figure B1 shows the three possible orientations of the F_A defects and indicates the optical dipole moments of the two absorption components F_{A_1} and F_{A_2}. Signals are recorded by inducing a population difference between orientations 1 and 2 in Fig. B1 (populations n_1 and n_2, with the dimension cm^{-2}). Only these two orientations are involved, since orientation 3 is symmetric to light incident from the left.

To induce the maximum imbalance between n_1 and n_2, the crystal must be exposed to light exclusively in the F_{A_1} or F_{A_2} bands, and the light must be polarized parallel to the appropriate optical moment. First consider exposure to vertically polarized F_{A_2} light. Defects in orientations 2 and 3 will rotate into orientation 1, and the equilibrium population distribution will become

$$n_1 = N, \quad n_2 = n_3 = 0, \tag{B1}$$

where N is the total concentration of defects. The crystal is now fully polarized. (This is an ideal case; in general the maximum degree of alignment rarely exceeds 90%.) If the incident F_{A_2} light polarization is now rotated 45° so as to have equal projections on the 1 and 2 orientations, the populations of 1 and 2 will equalize, and at equilibrium the polarizing property is lost. Calculations with the aid of Fig. A1 shows that at equilibrium the population distribution becomes

$$n_1 = n_2 = 2N/5, \quad n_3 = N/5. \tag{B2}$$

The distributions B1 and B2 may be cycled indefinitely by switching the F_{A_2} light polarization between vertical and 45°.

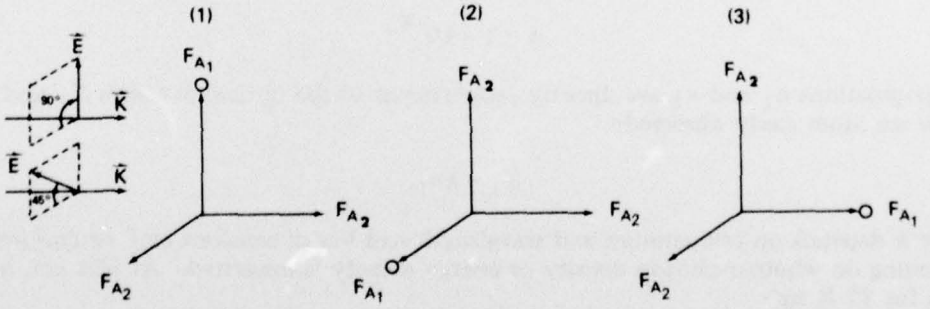

Fig. B1 — The three possible orientations of the F_A defect, showing the corresponding optical dipole moments of the F_{A_1} and F_{A_2} bands. Absorption of a photon by any of these orientations causes a rotation into one of the other two with an efficiency of 0.5.

Consider now the same operation using F_{A_1} light, which has only one dipole moment per orientation. In this case the population distribution becomes

$$n_1 = 0, \quad n_2 = n_3 = N/2. \tag{B3}$$

The crystal is again fully aligned (polarized) but with only half the population difference of the F_{A_2} excitation. A more significant difference between the two cases can be seen when the F_{A_1} light polarization is rotated 45°. Examination of Fig. B1 shows that at equilibrium the population distribution becomes

$$n_1 = n_2 = 0, \quad n_3 = N. \tag{B4}$$

Although n_1 and n_2 have been equilized and the polarizing property is lost, it has been done at the expense of driving all defects into orientation 3. Figure B1 shows that F_{A_1} light incident from the left cannot be absorbed by orientation 3. Thus, to realign n_1 relative to n_2 with F_{A_1} light, the crystal must be first exposed to F_{A_2} light. In summary, operation in the F_{A_2} band requires only a shift in polarization to cycle the polarizing property, but operation in F_{A_1} also requires an auxiliary F_{A_2} light source to drive centers out of orientation 3. Of course the latter could be any broadband light source. These population distributions are summerized in Table B1.

The preceding analysis deals only with equilibrium distributions, but the dynamic characteristics can be derived, at least for the simple case of F_{A_1} light. Assume the distribution of centers is random and vertically polarized light is incident from the left as indicated in Fig. B1. Let I be the photon density ($s^{-1}cm^{-2}$), and let A be the fraction of these photons absorbed by the population n_1 in orientation 1. Since the quantum efficiency for reorientation is 0.5, the rate of change of n_1 can be written

$$\dot{n}_1 = -IA(0.5). \tag{B5}$$

There is a probability of 0.5 that orientation 2 will gain any defect lost by orientation 1; therefore

$$\dot{n}_2 = IA(0.5)(0.5). \tag{B6}$$

The fraction of photons absorbed is

$$A = 1 - 10^{-K_1}. \tag{B7}$$

The populations n_1 and n_2 are directly proportional to the optical densities K_1 and K_2, which are more easily observed:

$$K_1 = kn_1, \tag{B8}$$

where k depends on temperature and wavelength and has dimensions cm^2 or cm^2/mJ, depending on whether photon density or energy density is measured. At 514 nm, k is given for 77 K by

$$k = 2.00 \times 10^{-16}\ cm^2 \tag{B9a}$$

and for 240 K by

$$k = 1.05 \times 10^{-16}\ cm^2. \tag{B9b}$$

Table B1 — Equilibrium Population Distributions of N Defects Oriented as Shown in Fig. A1

Excitation		Population Distribution		
Band	Polarization	n_1/N	n_2/N	n_3/N
F_{A_2}	Vertical	1	0	0
F_{A_2}	45°	2/5	2/5	1/5
F_{A_1}	Vertical	0	1/2	1/2
F_{A_1}	45°	0	0	0

Equations B5 and B6 now become

$$\dot{K}_1(E) = -\frac{1}{2} kI(1 - 10^{-K_1}) \tag{B10a}$$

and

$$\dot{K}_2(E) = \frac{1}{4} kI(1 - 10^{-K_1}), \tag{B10b}$$

where E is the exposure symbols. Equations B10 have the solutions

$$K_1(t) = \log [(10^{K_0} - 1)e^{-kIt/2} + 1] \tag{B11a}$$

and

$$K_2(t) = \frac{3}{2} K_0 - \frac{1}{2} K_1(t), \tag{B11b}$$

where K_0 is the initial optical density for 514 nm. Since It is the exposure, Eqs. B11 can be written

$$K_1(E) = \log [(10^{K_0} - 1)e^{-pE} + 1] \tag{B12a}$$

and

$$K_2(E) = \frac{3}{2} K_0 - \frac{1}{2} K_1(E), \tag{B12b}$$

where $p = k/2$ and has units of cm^2/mJ and E is expressed in mJ/cm^2. For 514-nm light there are 2.5×10^{15} photons/s per mW. Hence at 77 K, $p = 0.50$; and at 240 K, $p = 0.25$.

Appendix C

TRANSMISSION CHARACTERISTICS

Consider the situation depicted in Fig. C1. The incident light on the photodichroic crystal consists of an E vector with components a_1 and a_2 along the crystal axis:

$$\mathbf{E} = a_1\hat{\mathbf{i}} + a_2\hat{\mathbf{j}}. \tag{C1}$$

If the crystal has dichroism (the absorption constants K_1 and K_2 are different along each crystal axis), then the components a_1 and a_2 will experience a different attenuation as they propagate through the crystal, as illustrated in the upper part of Fig. C1. In addition to this effect there is also a birefringence induced by the dispersion effects of the dichroism. This latter effect can be calculated from the Kronig-Kramers dispersion relation

$$n_1(\omega) - n_2(\omega) = \frac{2\pi}{c}\int_0^\infty \frac{K_1(\omega') - K_2(\omega')}{\omega'^2 - \omega^2}\, d\omega', \tag{C2}$$

where n_1 and n_2 are the indices of refraction along the crystal axis and ω is the angular frequency. Computer calculations have shown that this effect can be appreciable for an optically anisotropic defect such as the F_A center. The dispersion effects are additive in the wavelength range between the two absorption bands and subtract in the wings. The index-of-refraction difference gives rise to a rotation of the components a_1 and a_2 in addition to their respective attenuations. This phase angle is

$$\delta = \frac{2\pi d(n_1 - n_2)}{\lambda}, \tag{C3}$$

where d is the crystal thickness. This effect is illustrated by the lower part of Fig. C1. Thus the E vector after propagating through the crystal can be written

$$\mathbf{E} = a_0[e^{-0.434K_1/2+i\delta/2}\hat{\mathbf{i}} + e^{-0.434K_2/2-i\delta/2}\hat{\mathbf{j}}] \tag{C4}$$

with

$$|\mathbf{E}(0)|^2 = I_0 = 2a_0^2 \tag{C5}$$

being the incident intensity. Consider the transmission of this E vector through the analyzer of Fig. C1. The normalized easy direction of this analyzer is

$$\mathbf{A} = \frac{1}{\sqrt{2}}(\hat{\mathbf{i}} - \hat{\mathbf{j}}). \tag{C6}$$

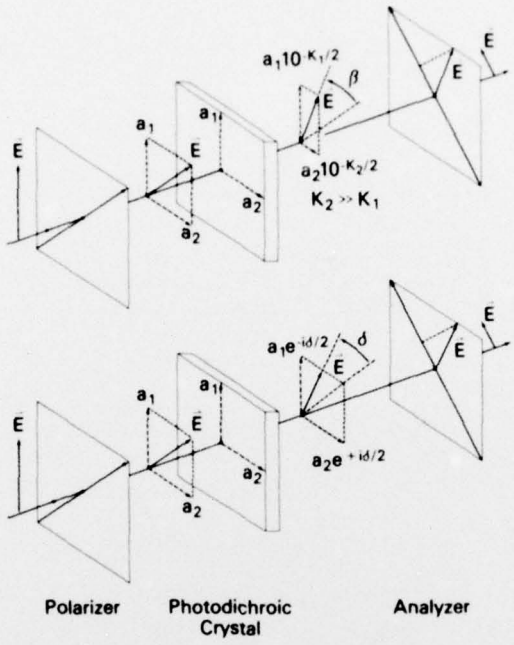

Fig. C1 — Attenuation and phase change in a photodichoric crystal. The upper part of the diagram illustrates the relative attenuation of the amplitude components a_1 and a_2 as they pass through the crystal. Amplitude a_1 sees an optical density of $K_1/2$, and a_2 sees $K_2/2$. If $K_2 >> K_1$ (there is dichroism), a_2 is greatly attenuated compared to a_1, which effectively rotates the E vector by some angle β given by $\beta = (\pi/4) - 10^{-(K_1 - K_2)/2}$. The lower part of the diagram illustrates the phase change experienced by the components a_1 and a_2 as they pass through the crystal due to the birefringence (given by B2). In general both effects are present.

The intensity transmission of light through the analyzer is then

$$I = |\mathbf{E}\cdot\mathbf{A}|^2$$

$$= 2a_0^2[(10^{-K_1/2} - 10^{-K_2/2})^2 + 10^{-(K_1+K_2)/2}\sin^2\delta/2]. \quad \text{(C7)}$$

Since the intensity transmission is given by I/I_0, this can be written

$$T = \frac{1}{4}(10^{-K_1/2} - 10^{-K_2/2})^2 + 10^{-(K_1+K_2)/2}\sin^2\delta/2. \quad \text{(C8)}$$